Published by
NIGERIAN SOCIETY OF PHYSICAL SCIENCES
Available online @ https://asr.nsps.org.ng/index.php/asr

African Scientific Reports 5 (2026) 444

African Scientific Reports

Bioelectrochemical transformation of synthetic waste from the Vaal region: effects of acetic acid, sugar, and salt on biogas production and electricity generation using a microbial fuel cell

Wato Nathan Fundji[a,*], Kitenge Marie Ngoie[b], Kabamba Arthur Makenda[c], John Kabuba[a]

[a]*Department of Chemical and Metallurgical Engineering, Faculty of Engineering and Technology, Vaal University of Technology, Private Bag X021, Andries Potgieter Blvd, Vanderbijlpark 1911, Gauteng, South Africa*
[b]*Department of Industrial Engineering, Operations Management and Mechanical Engineering, Faculty of Engineering and Technology, Vaal University of Technology, Private Bag X021, Andries Potgieter Blvd, Vanderbijlpark 1911, Gauteng, South Africa*
[c]*Department of Natural Sciences, Faculty of Applied and Computer Sciences, Vaal University of Technology, Private Bag X021, Andries Potgieter Blvd, Vanderbijlpark 1911, Gauteng, South Africa*

Abstract

This study investigated the effects of common domestic organic modifiers—acetic acid, brown sugar, and table salt—on the electrochemical, physicochemical, and bioenergetic characteristics of low-strength synthetic wastewater in a microbial fuel cell (MFC). Four wastewater matrices representing sewage from the Vaal region were prepared and maintained under anoxic conditions for 30 days. Maximum biogas production of 189 ppm and electrical output of 164 mV were recorded, indicating substrate-selective microbial activity. Fourier transform infrared spectroscopy (FTIR) confirmed structural changes in functional moieties in suspended solids and showed that salt and sugar were completely solubilized. Although biochemical oxygen demand (< 0.3 mg L^{-1}) and chemical oxygen demand (< 5 mg L^{-1}) were extremely low, the resident microbial communities remained electroactive, indicating that the MFC could recover energy even from matrices with low biodegradability. Response surface methodology (RSM) based on a central composite design (CCD) was used to model and optimize the effects of pH, exposure time, and substrate concentration on conductivity, total dissolved solids, and oxidation–reduction potential. Strong quadratic and interaction effects ($p < 0.0001$) indicated nonlinear interactions between redox potential and ionic strength. These findings suggest that low-cost additive strategies may improve MFC performance in dilute effluents from the Vaal region and support decentralized wastewater-to-energy applications.

DOI:10.46481/asr.2026.5.2.444

Keywords: Biogas, Microbial fuel cell, Vaal region, Wastewater

Article History:
Received: 11 January 2026
Received in revised form: 06 April 2026
Accepted for publication: 07 April 2026
Available online: 10 June 2026

*Corresponding author Tel. No.: +27 16 950 9887.
Email address: 214006166@edu.vut.ac.za (Wato Nathan Fundji)

1. Introduction

The need for clean and renewable energy is growing. Sustainable biological products, carbon capture, storage and reuse, and environmentally friendly energy-recovery technologies are being considered as part of the transition away from fossil fuels. Renewable energy is important for climate-change mitigation and energy security and can also benefit historically marginalized communities [1–5]. The application of microbial fuel cells (MFCs) offers several advantages, including high substrate-to-power conversion efficiency, recovery of valuable products, and reduction of sludge volume. However, although MFCs have been tested at industrial scale, important economic and operational challenges remain [6–8].

In MFCs, organic matter in the anaerobic anodic chamber is decomposed by microorganisms. Electrons generated during this process are captured at the anode and transferred through an external circuit to the cathode. At the cathode, electrons combine with oxygen and protons transported through an ion-exchange membrane, thereby producing electrical energy from the difference between anodic oxidation and cathodic reduction reactions [9–11]. Microorganisms also degrade diverse organic compounds and heavy-metal complexes while transferring electrons to electrodes. These microorganisms form biofilms on the electrode surface, which allows more efficient electron transfer than would occur with soluble electron acceptors. Biofilm formation on the anode is therefore a prerequisite for effective extracellular electron transfer [12–14].

Extracellular electron-transfer systems enable some microorganisms to survive in oxygen-limited environments by using insoluble electron acceptors. Two main MFC configurations are commonly used: two-chamber and single-chamber systems. The two-chamber design consists of anodic and cathodic compartments separated by an ion-exchange membrane, with one electrode in each chamber. In many designs, the ion-exchange membrane and cathode are in physical contact, with the cathode exposed directly to air [15–17]. Under these conditions, substrate selection, including glucose, acetate, synthetic wastewater, and real wastewater, strongly affects power density and microbiological stability over time [18–20].

Previous studies have shown that MFCs can extract energy while substantially reducing chemical oxygen demand (COD) [21, 22]. However, efficiency varies with operating parameters, including pH, temperature, and initial substrate concentration [23, 24]. Correlating physicochemical measurements, such as pH, conductivity, and oxidation–reduction potential (ORP), with microbiological measurements can help predict operational changes needed to maintain performance and stability [22, 25]. Although previous work has focused on reactor design, electrode materials, microbial-community optimization, and complex wastewater streams [19, 26, 27], less attention has been paid to the systematic influence of simple organic and ionic modifiers on MFC electrochemical behavior under controlled conditions. In particular, the effects of readily degradable substrates, such as sugars and organic acids, and ionic modifiers, such as salts, on conductivity, ORP, and total dissolved solids (TDS) remain insufficiently resolved. This study addresses that gap by combining controlled substrates (acetic acid, sugar, and salt) with response surface methodology (RSM) to evaluate their combined effects on electrochemical parameters, biogas production, and electricity generation in an MFC using synthetic wastewater representing the Vaal region.

2. Materials and methods

2.1. Materials and preparation of the microbial fuel cell

The MFC was constructed using components designed to generate bioelectricity through microbial activity, as shown in Figure 1. In Figure 1, cable was connected to the metallic mesh for a better stability and put in a tank (a); a bridge made of a salty piece of cord linking two tanks (b), both tanks were covered but wastewater filled one tank then passed to the other tank through the salty bridge (c), and the cables from tanks passing through their covers were connected to the probes of the multimeter and reading was made (d). Two polyvinyl chloride tanks were used as the anode and cathode chambers. Small holes were drilled near the top of the containers for electrical wiring. Carbon-based mesh electrodes were pretreated according to standard electrochemical cleaning procedures, and the wires were secured with electrical tape to ensure conductivity. Electrodes were placed in both chambers, and the drilled holes were sealed with hot glue to prevent leakage. The anode chamber was filled with wastewater containing mud from the Vaal region to provide a microbial inoculum, and the cathode chamber was filled with water from the anode chamber. The two chambers were connected by a salt bridge to enable the ion exchange required for electricity generation.

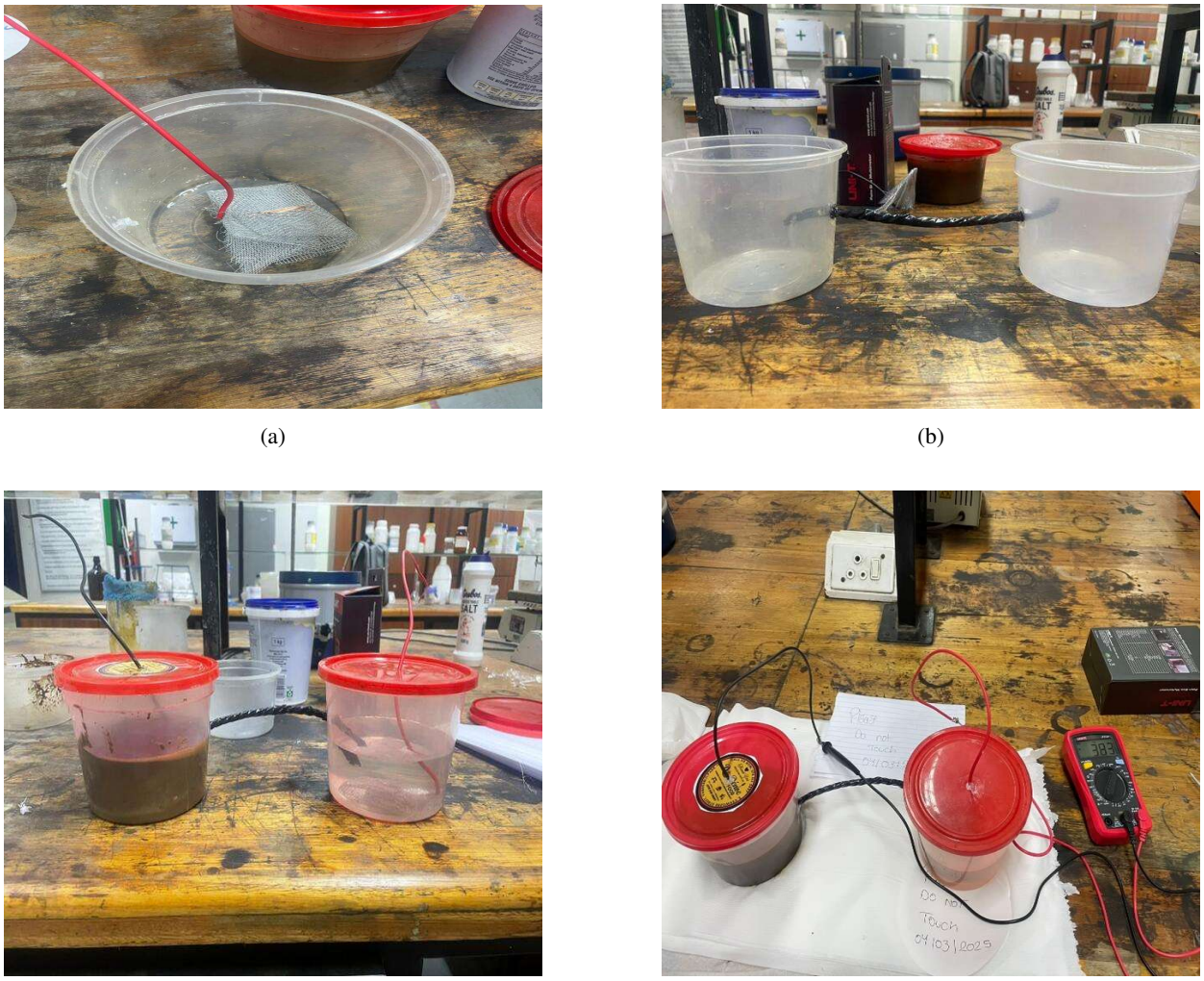

(a) (b)

(c) (d)

Figure 1: Preparation of one microbial fuel cell.

After assembly, microbial activity in the anode chamber generated electrons that were transferred to the steel mesh and measured using a multimeter.

TDS and electrical conductivity (EC) were measured using calibrated conductivity/TDS meters, and ORP was measured using a platinum ORP electrode with an accuracy of ±2 mV. Potassium hydroxide pellets (KOH, 99% pure), zinc chloride ($ZnCl_2$, 98% pure), and glacial acetic acid (CH_3COOH, 100% pure) were purchased from Aldrich (USA). $ZnCl_2$ solutions of 2.0, 1.5, and 1.0 M were prepared for the experimental trials, and KOH and CH_3COOH were used to adjust pH. Synthetic wastewater was prepared for biogas production and stored in four 1 L bottles for approximately 1.5 months. Each bottle contained 700 mL of tap water. Acetic acid (10 mL), sugar (50 g), and salt (50 g) were added separately to three containers. One container contained only water. Mango, a small piece of pork, and a small quantity of mud were added to all four bottles. The bottles were tightly sealed and secured with polyvinyl chloride electrical tape to prevent leakage.

2.2. Experimental design parameters using response surface methodology

A central composite design (CCD) within RSM was used to calculate the total number of experimental runs, as shown in Table 1. Analysis of variance was then used to evaluate the significance and suitability of the model.

Table 1: Parameters and their values.

Standard order	pH	Time (days)	Concentration (M)
1	7.00	1.00	1.50
2	7.00	2.00	1.50
3	5.00	3.00	2.00
4	7.00	3.00	1.50
5	5.00	1.00	2.00
6	7.00	2.00	1.50
7	7.00	2.00	1.50
8	7.00	2.00	1.50
9	7.00	2.00	1.50
10	5.00	2.00	1.50
11	9.00	1.00	1.00
12	5.00	3.00	1.00
13	7.00	2.00	1.50
14	9.00	1.00	2.00
15	9.00	3.00	1.00
16	5.00	1.00	1.00
17	9.00	3.00	2.00
18	7.00	2.00	2.00
19	7.00	2.00	1.00
20	9.00	2.00	1.50

3. Results and discussion

3.1. Fourier-transform infrared spectroscopy interpretation

Figure 2 shows the Fourier-transform infrared (FTIR) spectra of sugar, salt, and mud. In the sugar spectra, the polysaccharide fingerprint region was observed between 750 and 1200 cm^{-1}, with peaks at 850, 990, and 1020 cm^{-1} corresponding to α and β linkages in the polymer structure. The bands at 1250 and 1500 cm^{-1} were attributed to symmetric COO^- stretching vibrations. C–H stretching in methylene groups or overlapping O–H groups occurred at 2926 cm^{-1}. Absorption bands in the 3100–3600 cm^{-1} region indicated O–H groups associated with hydrogen bonding in the hydroxyl groups of glucopyranose rings [28].

FTIR analysis was also performed on salt particles to assess possible contaminant composition. The salt spectra showed absorption bands associated with commonly used synthetic polymers, with distinct peaks at 1710–1740 cm^{-1} (C=O stretching) and 1210–1000 cm^{-1} (C–O stretching) [29]. Changes in peak strength indicated variation in polymer concentration and possible compositional complexity. Overlapping absorption patterns in the 1000–1500 cm^{-1} region suggested the presence of multiple polymer types in individual samples. These findings suggest that the commercial salts used may have been contaminated by packaging or processing materials.

Three main spectral zones were distinguished in the original mud [30]. $N–H_2$ and O–H stretching vibrations from clay minerals and soil organic matter dominated the broad absorption bands between 2500 and 4000 cm^{-1}, with contributions from aromatic C–C, COO^-, and N–H vibrations. The sharp peak around 1000 cm^{-1} indicated Si–O–Si stretching in clay minerals and C–O stretching in polysaccharides. Some soils may also show characteristic mineral-related vibrations, such as an O–H stretching shoulder near 3500 cm^{-1}.

As shown in Figure 3 and Table 2, spectra for sugar and salt were not detected after the experiment. These substances were likely dissolved in the wastewater during the experiment.

3.2. Evaluation of physicochemical parameters

The results from the MFC experiments are presented in Table 3, which summarizes the effects of different synthetic wastewater compositions on physicochemical parameters and biogas production.

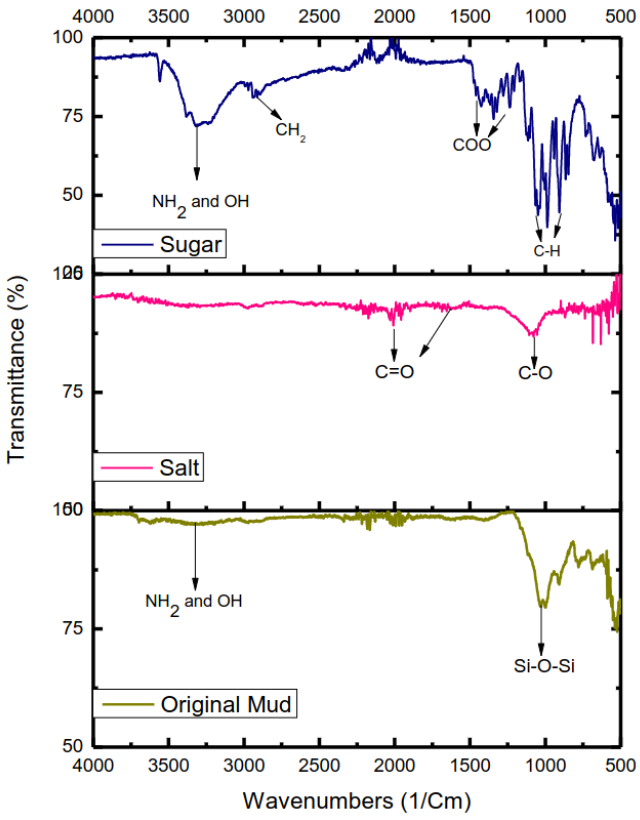

Figure 2: FTIR spectra of the original mud, salt, and sugar.

Table 2: Interpretation of FTIR changes in the mud samples.

Wavenumber (cm^{-1})	Functional group	Observation
3700–3200	O–H stretching	Hydroxyl groups associated with clay minerals, such as kaolinite, and adsorbed water. A broad band was observed in both the initial and after-experiment samples, indicating residual moisture and surface hydroxyl groups. A slight decrease in band intensity suggested water loss or partial dehydroxylation of the clay matrix [30].
2920–2850	C–H stretching	Aliphatic hydrocarbons and related organic matter. The lower intensity after the experiment indicated possible degradation or elimination of organic constituents [31].
1650–1630	H–O–H bending	Adsorbed water and organic compounds. Lower intensity after the experiment suggested reduced water content or decomposition of organic matter [32].
1450–1380	C–O stretching; O–H deformation	Carbonates or organic acids. Peak attenuation or displacement may have resulted from mineral transformation or gradual CO_2 release during the assay [33].
1100–1000	Si–O–Si stretching	Silicate minerals, including clays, quartz, and feldspar. A strong persistent band in both samples indicated that the primary silicate framework remained structurally intact during the experiment [34].
800–500	Si–O–Al and Si–O–Mg bending	Clay-mineral constituents. Small changes may be associated with cation-exchange processes or slight rearrangement of the silicate network [35].

The wastewater based on rotten fruit and meat was exposed to different additives (salt, sugar, and acetic acid) and stored for 30 days. The pH values ranged from 3.46 to 3.68, indicating consistently acidic conditions. Most methanogenic archaea are inhibited below approximately pH 4.0, and many methanogens generally require neutral to weakly alkaline conditions (pH 6.5–8.0) [36]. However, acid-tolerant microbial communities can adapt and perform anaerobic digestion, although often with lower methane yields or altered biogas composition [37]. The acetic acid sample had a slightly higher pH than the other samples, which may be related to its role as an intermediate in methanogenesis, where consumption can slightly increase pH if buffering capacity is present [38].

The ORP values ranged from 86 to 147 mV. Lower ORP values generally indicate more reducing conditions,

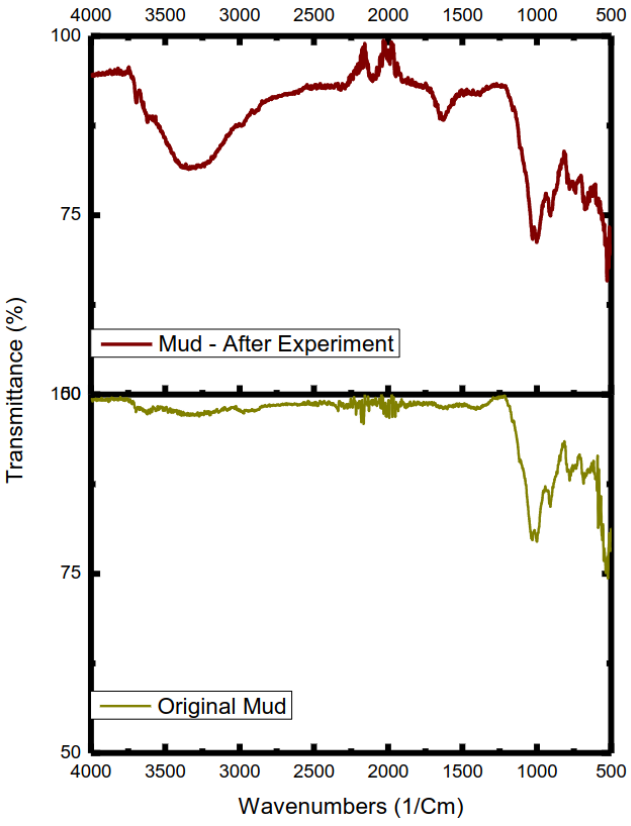

Figure 3: Changes observed in the FTIR spectra of the mud.

Table 3: Results obtained from MFC experiments based on the type of synthetic wastewater.

Parameter	Wastewater only	Salt	Sugar	Acetic acid
pH	3.49	3.46	3.53	3.68
ORP (mV)	113	144	86	147
Conductivity (μS cm^{-1})	2530	49.4	2060	1900
TDS (ppm)	1260	25.9	1030	959
BOD (mg L^{-1})	< 0.3	< 0.3	< 0.3	< 0.3
COD (mg L^{-1})	< 5	< 5	< 5	< 5
Total coliforms	Present	Present	Present	Present
Biogas (ppm)	175	189	130	59

which can favor anaerobic processes, including methanogenesis [39, 40]. The sugar sample had the lowest ORP, suggesting a strongly reduced environment, probably resulting from rapid sugar fermentation and electron-acceptor depletion [41, 42]. High conductivity and TDS may inhibit microbial activity, particularly methanogens, because of osmotic stress and enzyme inhibition [43, 44]. The wastewater-only sample had the highest conductivity and TDS, indicating a high concentration of dissolved ions from the rotten fruit and meat feedstock. Unexpectedly, the salt sample had the lowest conductivity and TDS. This result suggests that the table-salt addition did not produce the expected high ionic strength, or that other matrix effects affected the conductivity measurements. High wastewater salinity can reduce biogas production and alter microbial communities.

All samples had extremely low biochemical oxygen demand (BOD; < 0.3 mg L^{-1}) and COD (< 5 mg L^{-1}).

Table 4: Electrical readings for the different MFC wastewater treatments.

Treatment	Data collection time	Voltage (mV)	Resistance (MΩ)	Current (μA)
Mud with salt	Day 1	0	0	0
	Day 2	-9	0.7	0
	Day 3	12	1.2	0.02
	Day 4	-5	0	0
Mud with acetic acid	Day 1	8	0	0.30
	Day 2	40	0	0.02
	Day 3	14	0	0.52
	Day 4	164	0.8	0.49
Mud with sugar	Day 1	0	0	0
	Day 2	87	0.3	0.39
	Day 3	155	0.6	0.047
	Day 4	164	0.8	0.49
Mud with wastewater only	Day 1	0	0	0
	Day 2	125	0.6	0.38
	Day 3	127	0.6	0.40
	Day 4	130	0	0.37

Table 5: Analysis of variance for TDS.

Source	Sum of squares	DF	Mean square	F value	Prob. > F
Model	1.528×10^{14}	9	1.697×10^{13}	23.23	< 0.0001
A	4.923×10^{13}	1	4.923×10^{13}	67.37	< 0.0001
B	2.942×10^{13}	1	2.942×10^{13}	40.26	< 0.0001
C	1.847×10^{11}	1	1.847×10^{11}	0.25	0.6260
A^2	3.599×10^{13}	1	3.599×10^{13}	49.25	< 0.0001
B^2	2.048×10^{12}	1	2.048×10^{12}	2.80	0.1251
C^2	1.571×10^{12}	1	1.571×10^{12}	2.15	0.1733
AB	3.310×10^{13}	1	3.310×10^{13}	45.29	< 0.0001
AC	1.458×10^{9}	1	1.458×10^{9}	1.995×10^{-3}	0.9653
BC	3.277×10^{10}	1	3.277×10^{10}	0.045	0.8366
Residual	7.308×10^{12}	10	7.308×10^{11}	–	–
Lack of fit	5.526×10^{12}	5	1.105×10^{12}	3.10	0.1199
Pure error	1.782×10^{12}	5	3.565×10^{11}	–	–
Cor total	1.601×10^{14}	19	–	–	–

Std. dev.	8.549×10^{5}	R^2	0.9543
Mean	2.198×10^{6}	Adjusted R^2	0.9133
CV (%)	38.90	Predicted R^2	0.7249
PRESS	4.403×10^{13}	Adequate precision	17.542

These low values suggest that readily biodegradable and oxidizable organic matter was consumed during the 30 day storage period. In anaerobic digestion, higher influent BOD and COD typically indicate greater potential for biogas production [27, 45, 46]. The low BOD/COD values, together with measured biogas production, may indicate that biogas was generated from more recalcitrant organic matter or that measurements were taken after substantial degradation had already occurred [22, 25]. Total coliforms were present in all samples and may have participated in initial acidogenic processes [14, 26].

Biogas production varied considerably among samples. The salt sample produced the highest measured biogas

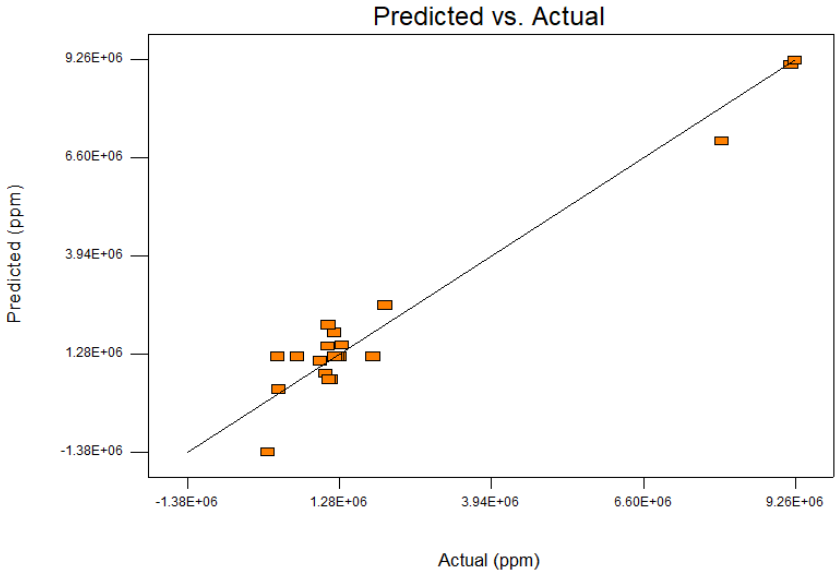

Figure 4: Predicted versus actual plot for the TDS response.

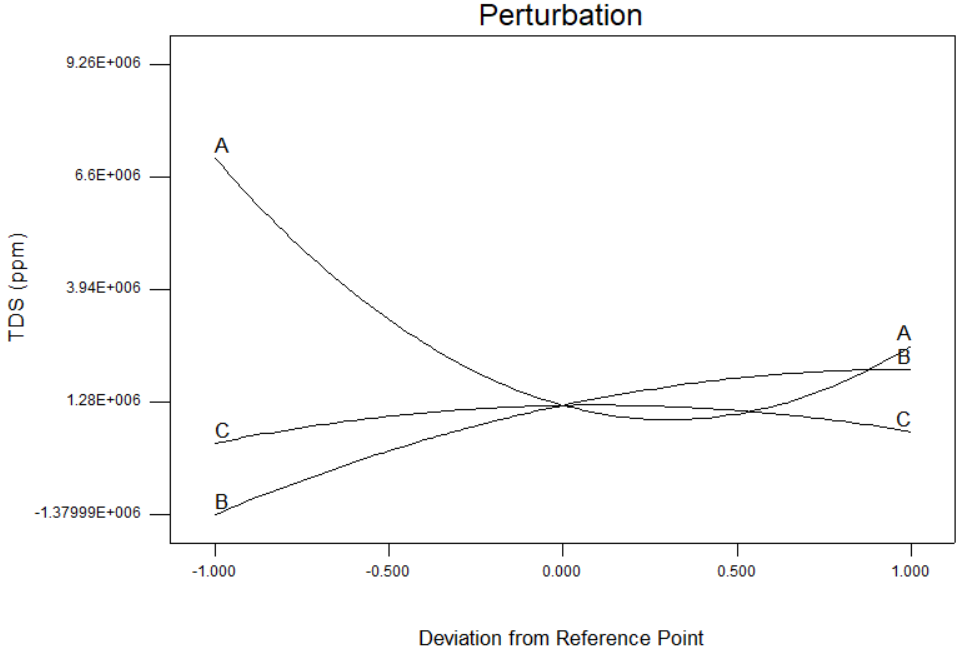

Figure 5: Perturbation plot for the TDS response.

concentration (189 ppm), despite its low conductivity and TDS. This could indicate that the salt addition optimized the microbial environment or added trace components without causing osmotic stress [20, 47–49]. The acetic acid sample produced the lowest biogas concentration (59 ppm). This is counterintuitive because acetic acid is a precursor in acetoclastic methanogenesis; however, the acidic pH or acetic acid concentration may have inhibited acetoclastic methanogens. Wastewater-only and sugar samples produced intermediate biogas concentrations of 175 and 130 ppm,

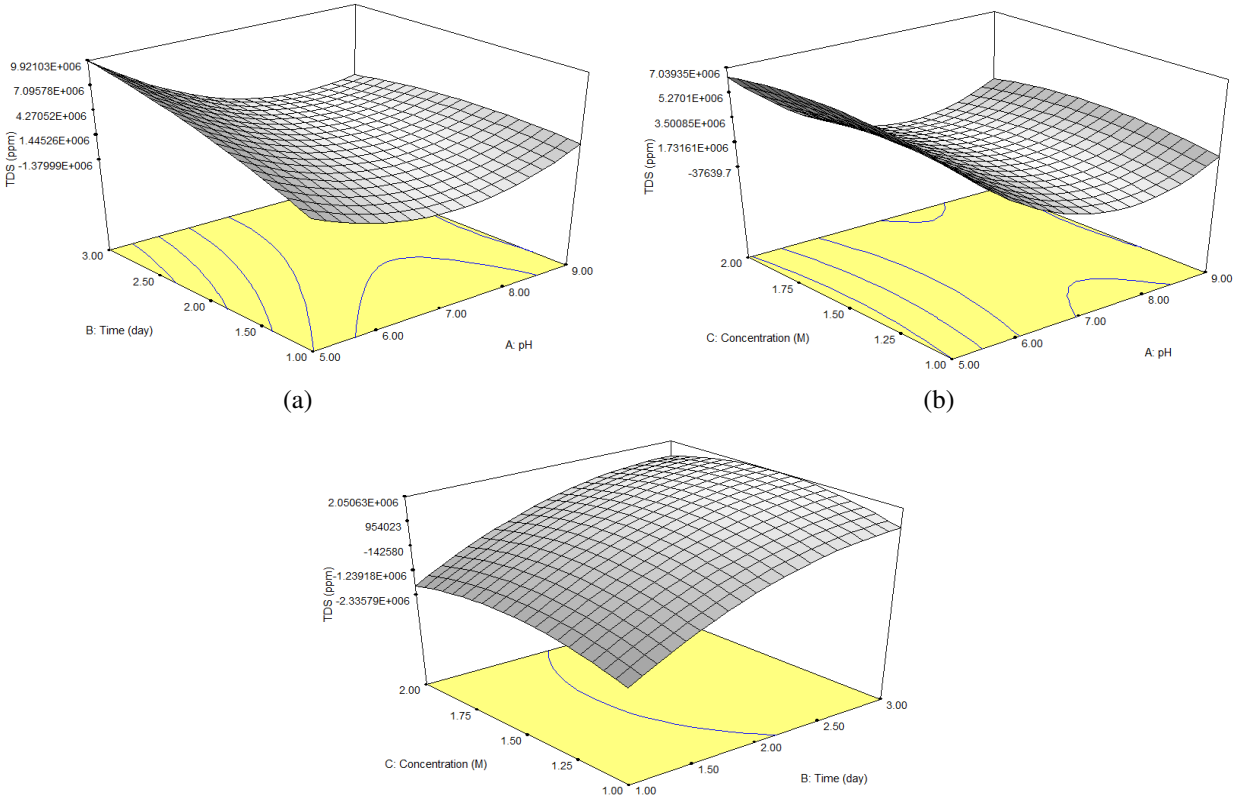

Figure 6: Three-dimensional response-surface plots for the TDS response versus two variables.

Table 6: Analysis of variance for conductivity.

Source	Sum of squares	DF	Mean square	F value	Prob. > F
Model	4.147×10^5	9	46079.87	28.79	< 0.0001
A	2.049×10^5	1	2.049×10^5	128.00	< 0.0001
B	2020.66	1	2020.66	1.26	0.2875
C	65910.04	1	65910.04	41.17	< 0.0001
A^2	20308.48	1	20308.48	12.69	0.0052
B^2	6645.82	1	6645.82	4.15	0.0689
C^2	7605.83	1	7605.83	4.75	0.0543
AB	7592.20	1	7592.20	4.74	0.0545
AC	80370.43	1	80370.43	50.21	< 0.0001
BC	4824.08	1	4824.08	3.01	0.1132
Residual	16008.22	10	1600.82	–	–
Lack of fit	14406.19	5	2881.24	8.99	0.0154
Pure error	1602.03	5	320.41	–	–
Cor total	4.307×10^5	19	–	–	–

Std. dev.	40.01	R^2	0.9628
Mean	124.55	Adjusted R^2	0.9294
CV (%)	32.12	Predicted R^2	0.5057
PRESS	2.129×10^5	Adequate precision	19.383

respectively, indicating that the original feedstock and sugar addition supported some anaerobic digestion. These results show the complexity of interactions among wastewater composition, pH, ORP, and microbial activity in biogas production.

3.3. Electrical values obtained

Table 4 summarizes the electrical performance of MFC systems with different wastewater compositions.

The substrates produced different voltage, resistance, and current profiles over the four monitored days. The sugar and acetic acid samples produced the highest voltage output (164 mV), suggesting increased microbial activity and improved electron transfer. Stable but lower outputs were obtained for the raw wastewater/control MFC, indicating that substrate enrichment influenced electrochemical performance. The intervals between Day 1 and Day 2, Day 2 and Day 3, including Day 3 and Day 4 were all equally 24 h. Day 1 corresponded to the day on which the MFCs were assembled and readings were collected immediately.

Electrical measurements for the four mud-MFC treatments showed no measurable voltage or current on Day 1, followed by electroactivity between Days 2 and 4 as the anode biofilm developed. The computed instantaneous power output was in the nanowatt range. The most stable performance was observed in wastewater-fed MFCs, which produced 47–51 nW (125–130 mV and 0.37–0.40 μA) between Days 2 and 4. Transient peaks reached approximately 80 nW on Day 4 (164 mV and 0.49 μA). The low output may have resulted from low organic content in the synthetic feedstock, limited electroactive microbial enrichment in the anode chamber, high internal resistance, and the small electrode surface area used in the laboratory-scale system. These observations are consistent with known MFC behavior: a lag phase associated with biofilm formation and enrichment of exoelectrogens, rapid electron transfer in the presence of readily degradable substrates such as acetate and glucose, and stable operation on mixed wastewater substrates that support a diverse electron-donating community [36, 50]. The near-zero performance of the salt-amended reactor was probably due to saline inhibition, which outweighed any benefit from enhanced ionic conductivity [23, 24]. The measured resistance values were obtained using a digital multimeter and represent instrument-measured resistance, not an external resistor applied for power optimization. The megaohm-range resistance accounts for the low measured currents in the microampere to nanoampere range and the small power output [51, 52]. Table 4 shows that substrate type had a significant effect on both the magnitude and stability of bioelectricity generation in MFCs.

3.4. Statistical studies

3.4.1. Total dissolved solids

The coded and actual equations for TDS are given in equations (1) and (2), respectively:

$$\begin{aligned}\mathrm{TDS} = {} & 1.198 \times 10^6 - 2.219 \times 10^6 A + 1.715 \times 10^6 B + 1.359 \times 10^5 C \\ & + 3.618 \times 10^6 A^2 - 8.629 \times 10^5 B^2 - 7.559 \times 10^5 C^2 \\ & - 2.034 \times 10^6 AB + 13500.00 AC - 64000.00 BC.\end{aligned} \tag{1}$$

$$\begin{aligned}\mathrm{TDS} = {} & 2.47064 \times 10^7 - 1.17573 \times 10^7 \mathrm{pH} + 1.24781 \times 10^7 \mathrm{Time} \\ & + 9.50399 \times 10^6 \mathrm{Concentration} + 9.04402 \times 10^5 \mathrm{pH}^2 \\ & - 8.62941 \times 10^5 \mathrm{Time}^2 - 3.02356 \times 10^6 \mathrm{Concentration}^2 \\ & - 1.01700 \times 10^6 \mathrm{pH} \times \mathrm{Time} + 13500.00000 \mathrm{pH} \times \mathrm{Concentration} \\ & - 1.28000 \times 10^5 \mathrm{Time} \times \mathrm{Concentration}.\end{aligned} \tag{2}$$

Overall, the quadratic model for TDS was statistically significant (F = 23.23, $p < 0.0001$; Table 5). The linear factors pH (A) and time (B), the pH quadratic term (A^2), and the interaction term AB were significant ($p < 0.0001$). The concentration factor (C) had no significant linear effect ($p = 0.6260$). The adequate precision value of 17.542 was well above the recommended value of 4, indicating a good signal-to-noise ratio. The lack-of-fit test was not significant ($p = 0.1199$), indicating that the quadratic model adequately fitted the data. However, the coefficient of variation (CV = 38.90%) indicated high experimental variability. Equation (1) shows a negative linear effect of pH and a positive quadratic effect, suggesting a TDS minimum near the middle of the tested pH range. Time had a strong positive linear effect, and the pH–time interaction indicated that the effect of time depended strongly on pH.

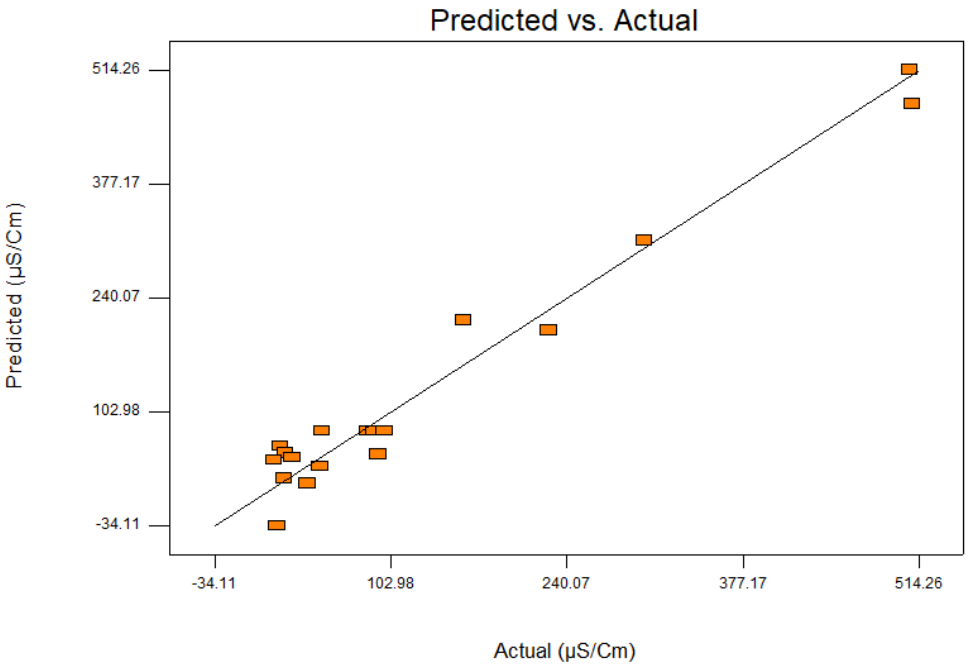

Figure 7: Predicted versus actual plot for the conductivity response.

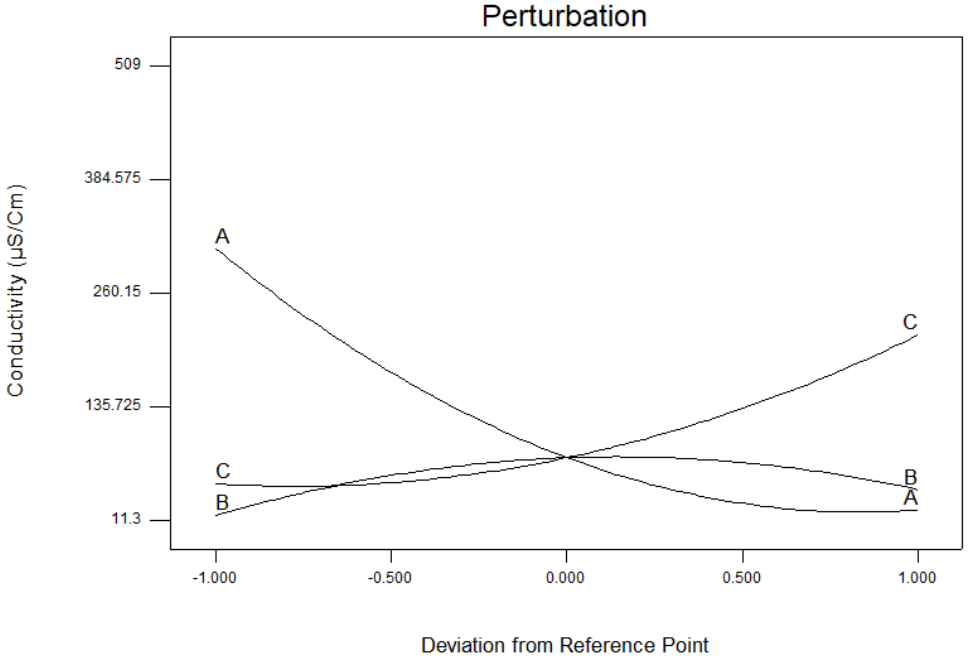

Figure 8: Perturbation plot for the conductivity response.

As shown in Figure 4, the predicted and actual TDS values clustered close to the 45° diagonal, indicating a good model fit with low variance. The close agreement between predicted and observed values was consistent with the high coefficient of determination ($R^2 > 0.95$). The perturbation plot in Figure 5 shows that factor A (pH) had the largest

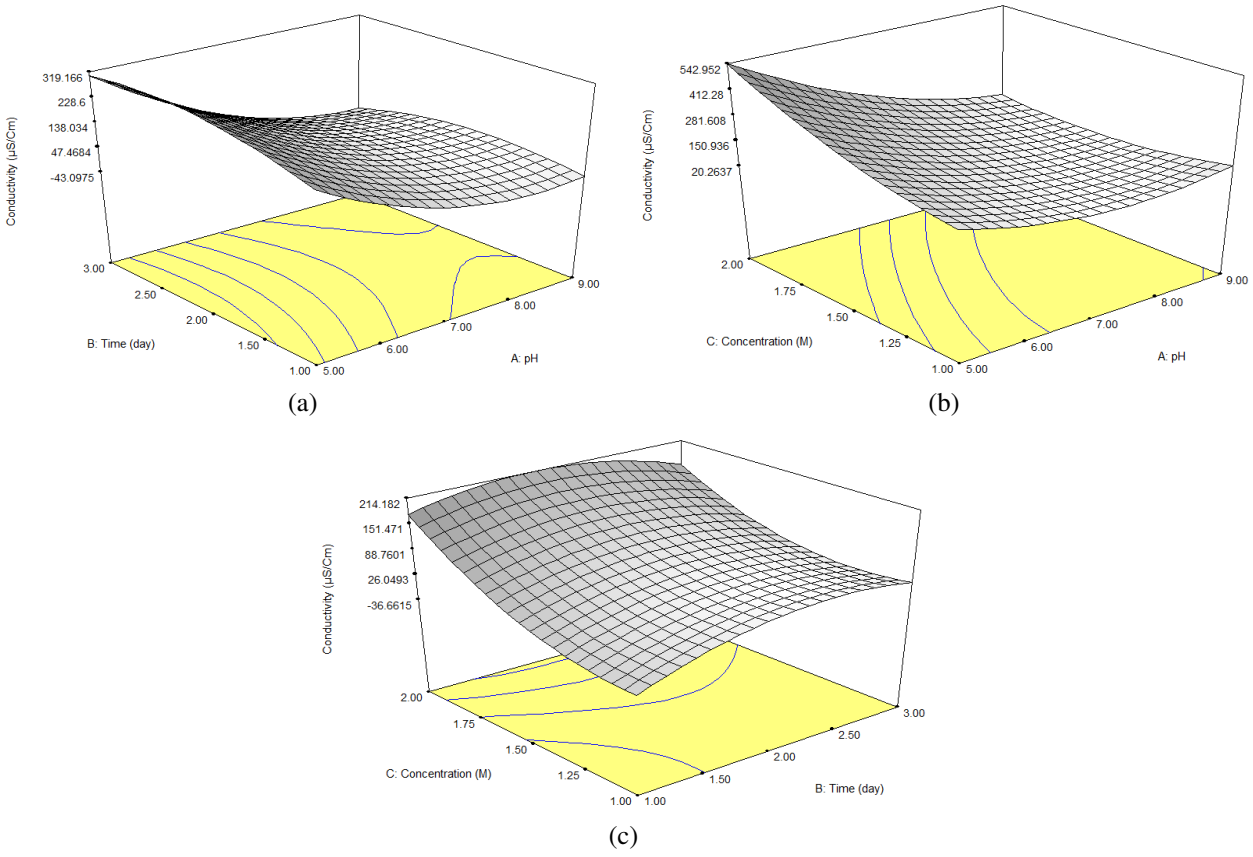

Figure 9: Three-dimensional response-surface plots for conductivity versus two variables.

Table 7: Analysis of variance for ORP.

Source	Sum of squares	DF	Mean square	F value	Prob. > F
Model	7.774×10^5	9	86372.93	26.80	< 0.0001
A	64000.00	1	64000.00	19.86	0.0012
B	2.091×10^5	1	2.091×10^5	64.88	< 0.0001
C	76912.90	1	76912.90	23.86	0.0006
A^2	12012.02	1	12012.02	3.73	0.0824
B^2	52440.02	1	52440.02	16.27	0.0024
C^2	1775.46	1	1775.46	0.55	0.4750
AB	253.13	1	253.13	0.079	0.7850
AC	25651.13	1	25651.13	7.96	0.0181
BC	2.574×10^5	1	2.574×10^5	79.87	< 0.0001
Residual	32229.35	10	3222.94	–	–
Lack of fit	14703.35	5	2940.67	0.84	0.5741
Pure error	17526.00	5	3505.20	–	–
Cor total	8.096×10^5	19	–	–	–

Std. dev.	56.77	R^2	0.9602
Mean	245.25	Adjusted R^2	0.9244
CV (%)	23.15	Predicted R^2	0.7985
PRESS	1.631×10^5	Adequate precision	18.249

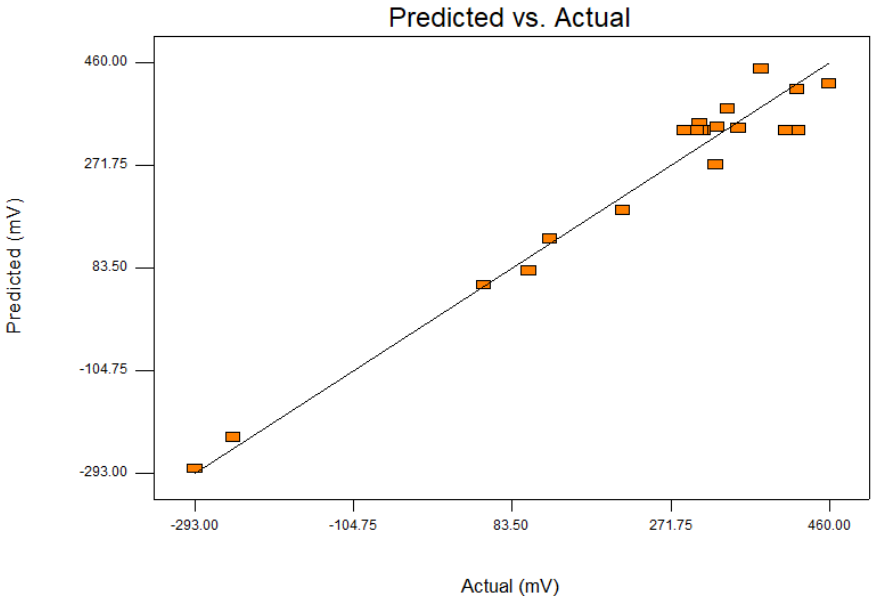

Figure 10: Predicted versus actual plot for the ORP response.

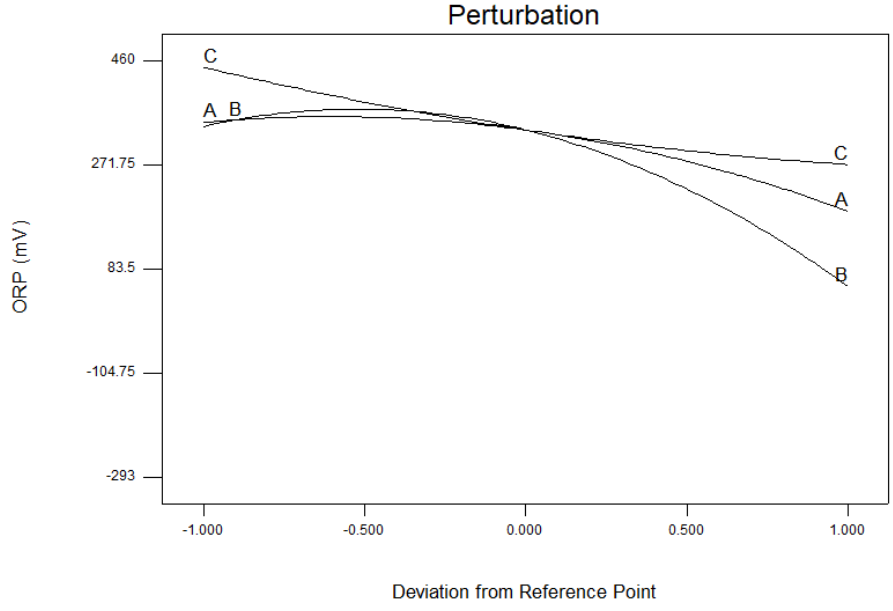

Figure 11: Perturbation plot for the ORP response.

effect on TDS, followed by factor B (time), whereas factor C (concentration) had the smallest effect. The steepness of factor A indicates that pH was important in regulating the electrolyte composition, which may be directly related to ionic transport and internal resistance in the MFC. TDS was sensitive to changes in conductivity and pH, suggesting that ionic strength and acid–base conditions strongly influenced solute build-up in the system. Similar trends have been observed in bioelectrochemical systems in which ion movement and internal resistance are linked to conductivity [23].

Figure 6 presents three-dimensional response-surface plots showing the interactive effects of paired variables on TDS while the third variable was held constant. In Figure 6, panel (a) describes the effect of pH and time on TDS,

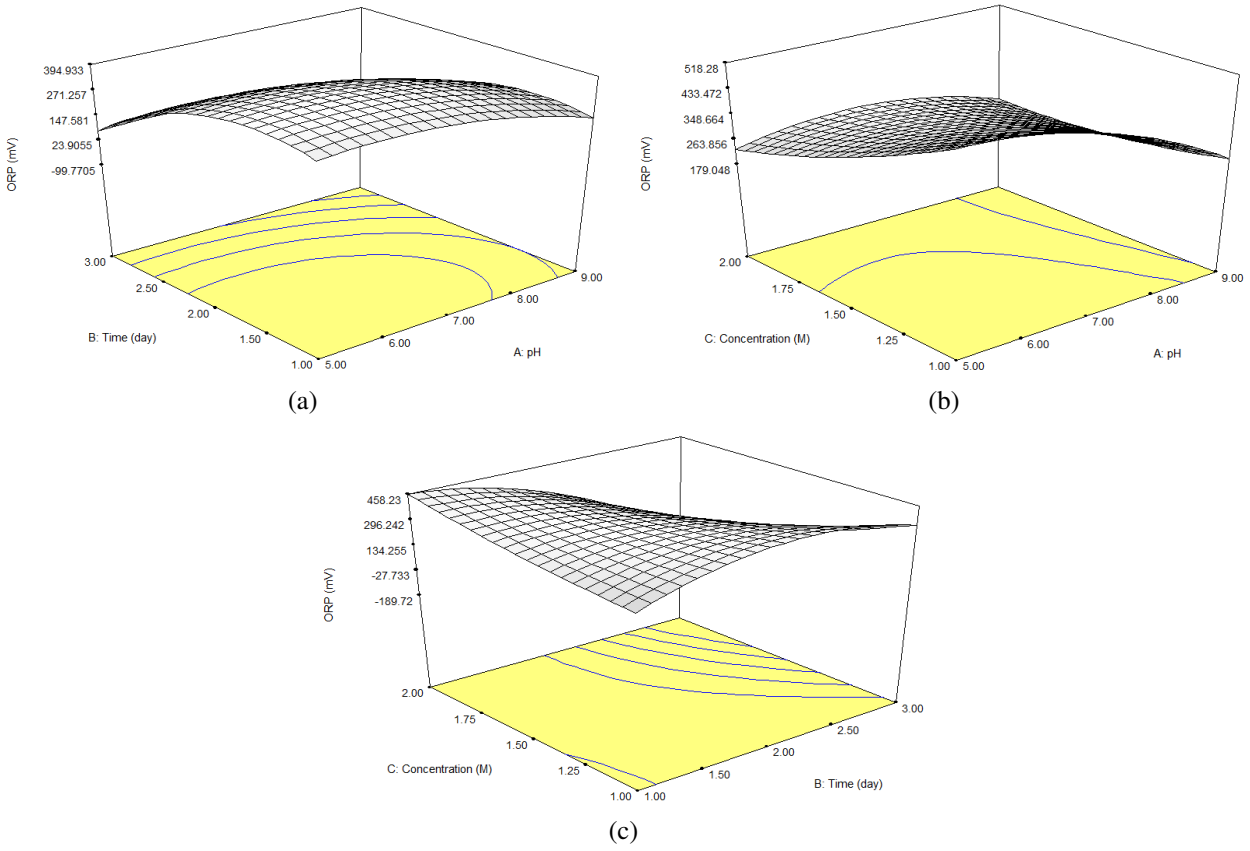

Figure 12: Three-dimensional response-surface plots for ORP versus two variables.

panel (b) describes the effect of pH and Concentration on TDS and panel (c) describes the effect of Time and concentration on TDS. Curvature in the response surfaces indicates nonlinear interactions among pH, conductivity, and operating time. A ridge was observed at moderate pH and conductivity, which may indicate an ionic environment that maximizes solute release without substantial precipitation. Such interactions are typical of MFCs, where electrochemical processes and microbial activity are controlled by multiple physicochemical parameters [23, 53].

3.4.2. Conductivity

The coded and actual equations for conductivity are given in equations (3) and (4), respectively:

$$\begin{aligned}\text{Conductivity} = {} & 79.86 - 143.15A + 14.22B + 81.18C + 85.94A^2 \\ & - 49.16B^2 + 52.59C^2 - 30.81AB - 100.23AC - 24.56BC.\end{aligned} \tag{3}$$

$$\begin{aligned}\text{Conductivity} = {} & 222.86567 - 191.19397\text{pH} + 392.34381\text{Time} \\ & + 331.12830\text{Concentration} + 21.48386\text{pH}^2 - 49.15955\text{Time}^2 \\ & + 210.36182\text{Concentration}^2 - 15.40312\text{pH} \times \text{Time} \\ & - 100.23125\text{pH} \times \text{Concentration} - 49.11250\text{Time} \times \text{Concentration}.\end{aligned} \tag{4}$$

The conductivity quadratic model was globally significant (F = 28.79, $p < 0.0001$; Table 6). Linear effects of pH (A) and concentration (C), as well as the pH–concentration interaction (AC), were significant ($p < 0.0001$). The time factor (B) was not linearly significant ($p = 0.2875$), although moderate quadratic effects were observed. The adequate precision value of 19.383 indicated good discriminatory power. The lack-of-fit test was significant ($p = 0.0154$),

suggesting that the quadratic model did not capture all systematic variability and that additional variables, transformations, or a broader model form may be required. The CV was 32.12%, indicating high variability. Equation (3) shows a strong negative linear effect of pH and a positive quadratic term, indicating a nonlinear relationship. Concentration had a positive coefficient, whereas the AC interaction was strongly negative, showing that conductivity increased with concentration differently across pH levels.

Figure 7 compares predicted and actual conductivity values, showing that the RSM model can estimate ionic conductance in the MFC system. The high degree of agreement supports the model fit ($R^2 = 0.96$) and indicates that conductivity variation was well explained by changes in TDS and pH [54, 55]. The perturbation plot in Figure 8 shows that factors A (pH) and C (concentration) influenced conductivity more strongly than factor B (time). The sharper curves for A and C indicate that conductivity was more responsive to these variables. This is important because electrolyte conductivity directly affects electron-transfer efficiency and internal resistance in MFC systems. Conductivity showed high sensitivity to TDS, consistent with the relationship between ion concentration and conductance. Its moderate sensitivity to pH may be associated with proton mobility and ionic speciation [23].

Figure 9 shows response-surface plots for the combined effects of variable pairs on conductivity. In Figure 9, panel (a) shows the effect of pH and time on Conductivity, panel (b) shows the effect of pH and Concentration on Conductivity and panel (c) shows the effect of Time and concentration on Conductivity. The curvature shows interactions and regions of maximum ionic conductance. Conductivity generally increased with TDS and operating time until a saturation level was reached, after which precipitation or clustering may have reduced conductance. Ion dissociation was pH dependent, and the pH–TDS interaction was strong. The observed peaks corresponded to conditions that may promote electron mobility and reduce internal resistance [23].

3.4.3. Oxidation–reduction potential

The coded and actual equations for ORP are given in equations (5) and (6), respectively:

$$\begin{aligned}\mathrm{ORP} = {} & 334.64 - 80.00A - 144.60B - 87.70C - 66.09A^2 \\ & - 138.09B^2 + 25.41C^2 - 5.62AB + 56.63AC - 179.38BC.\end{aligned} \tag{5}$$

$$\begin{aligned}\mathrm{ORP} = {} & -487.42159 + 112.00568\mathrm{pH} + 965.57614\mathrm{Time} \\ & - 159.18409\mathrm{Concentration} - 16.52273\mathrm{pH}^2 - 138.09091\mathrm{Time}^2 \\ & + 101.63636\mathrm{Concentration}^2 - 2.81250\mathrm{pH} \times \mathrm{Time} \\ & + 56.62500\mathrm{pH} \times \mathrm{Concentration} - 358.75000\mathrm{Time} \times \mathrm{Concentration}.\end{aligned} \tag{6}$$

The ORP model was globally significant ($F = 26.80$, $p < 0.0001$; Table 7). The primary effects of pH (A), time (B), and concentration (C) were significant. The B^2, AC, and BC interaction terms also contributed significantly. The lack-of-fit test was not significant ($p = 0.5741$), indicating that the model described the ORP response satisfactorily within the tested range. The CV of 23.15% was lower than for the other responses, indicating better repeatability. Equation (5) shows negative linear effects for pH, time, and concentration. The strongest interaction was BC, indicating that the effect of time on ORP depended strongly on concentration.

Figure 10 shows predicted and experimental ORP values from the RSM model. The near-linear relationship indicates that the model adequately explains redox variation. Because ORP is a direct response to microbial electron-transfer dynamics, the strong model fit suggests consistent electrochemical regulation [7, 56]. The perturbation plot in Figure 11 shows that factor B (time) had the greatest effect, followed by factor A (pH), whereas factor C (concentration) had the least steep effect within the experimental range. The high gradients of A and B indicate their importance in controlling oxidation–reduction processes that govern microbial metabolism and electron transfer. The perturbation analysis indicates that ORP was most affected by pH and conductivity, with a secondary effect of time. Maintaining optimum pH may therefore support more consistent bioenergy conversion [57].

The three-dimensional surfaces in Figure 12 show interaction effects of pH, conductivity, and operating time on ORP. In Figure 12, panel (a) shows the effect of pH and time on ORP, panel (b) shows the effect of pH and Concentration on ORP and panel (c) shows the effect of Time and concentration on ORP. Valleys and peaks indicate regions of decreasing and increasing potential, respectively. The strong curvature of the surfaces shows that redox dynamics in the MFC system were controlled by synergistic interactions between pH and conductivity. RSM identification of

these redox regions can guide the maintenance of microbial efficiency and electrode-potential balance [58]. TDS and ORP models were statistically robust, with no significant lack of fit, and may therefore be used for optimization within the tested range. However, the conductivity model showed significant lack of fit and should be refined before it is used for scale-up or external prediction [53, 59, 60].

4. Conclusion

This study determined the effects of acetic acid, sugar, and salt additives on biogas and electricity generation from synthetic wastewater using microbial fuel cells. The results showed a strong positive relationship between TDS and conductivity, with higher TDS observed under acidic conditions (pH 5) than under neutral and alkaline conditions. Conductivity was strongly correlated with TDS, indicating increased ion mobility and reduced ohmic resistance in the anode chamber. The CCD-based physicochemical adjustments showed that ionic mobility and redox stability can be improved in a two-chamber MFC operating with waste materials from the Vaal region. The main variables influencing TDS, conductivity, and ORP were pH and concentration, even at extremely low BOD levels. The steep perturbation curves indicate that the experimental variables strongly affected the electrochemical environment of the system, especially ionic concentration and redox conditions, which are important parameters controlling electron transfer and overall MFC performance.

Data availability

All data generated or analyzed in this study are included in this article. Additional datasets are available from the corresponding author upon reasonable request.

Declaration of competing interest

The authors declare that they have no known competing financial interests or personal relationships that could have appeared to influence the work reported in this paper.

Funding

The authors received no external funding for this study.

References

[1] N. Bazina, T. G. Ahmed, M. Almdaaf, S. Jibia & M. Sarker, “Power generation from wastewater using microbial fuel cells: A review”, Journal of Biotechnology **374** (2023) 17. https://doi.org/10.1016/j.jbiotec.2023.07.006.

[2] S. M. Daud, Z. Z. Noor, N. S. A. Mutamim, N. H. Baharuddin, A. Aris, A. N. M. Faizal, R. S. Ibrahim & N. S. Suhaimin, “A critical review of ceramic microbial fuel cell: Economics, long-term operation, scale-up, performances and challenges”, Fuel **365** (2024) 131150. https://doi.org/10.1016/j.fuel.2024.131150.

[3] P. Jalili, A. Ala, P. Nazari, B. Jalili & D. D. Ganji, “A comprehensive review of microbial fuel cells considering materials, methods, structures, and microorganisms”, Heliyon **10** (2024) e25439. https://doi.org/10.1016/j.heliyon.2024.e25439.

[4] R. S. Pandya, T. Kaur, R. Bhattacharya, D. Bose & D. Saraf, “Harnessing microorganisms for bioenergy with microbial fuel cells: Powering the future”, Water-Energy Nexus **7** (2024) 1. https://doi.org/10.1016/j.wen.2023.11.004.

[5] N. Rathinavel, A. Veleeswaran, Y. Rathinam & A. Alagarsamy, “Turning waste into watt: Usage of natural biomass activated carbon-based anode and septic tank wastewater for microbial fuel cell (MFC) based electricity generation”, Carbon Trends **19** (2025) 100461. https://doi.org/10.1016/j.cartre.2025.100461.

[6] S. Goel, “From waste to watts in micro-devices: Review on development of membraned and membraneless microfluidic microbial fuel cell”, Applied Materials Today **11** (2018) 270. https://doi.org/10.1016/j.apmt.2018.03.005.

[7] P. V. Nidheesh, S. O. Ganiyu, C. Kuppam, E. Mousset, N. Samsudeen, H. Olvera-Vargas & G. Kumar, “Bioelectrochemical cells as a green energy source for electrochemical treatment of water and wastewater”, Journal of Water Process Engineering **50** (2022) 103232. https://doi.org/10.1016/j.jwpe.2022.103232.

[8] D. Bose, R. Bhattacharya, M. Gopinath, A. Sarkar, R. S. Pandya & A. Jaiswal, “Advances in microbial fuel cell technologies for bioremediation and energy recovery from wastewater”, Sustainable Chemistry for the Environment **11** (2025) 100266. https://doi.org/10.1016/j.scenv.2025.100266.

[9] A. Mahmoudi, S. A. Mousavi & P. Darvishi, "Performance and recent development in sewage sludge-to-bioenergy using microbial fuel cells: A comprehensive review", International Journal of Hydrogen Energy **50** (2024) 1432. https://doi.org/10.1016/j.ijhydene.2023.10.338.

[10] C. Montoya-Vallejo, J. C. Quintero Díaz, Y. A. Yepes & F. J. Fernández-Morales, "Microalgal microbial fuel cells: A comprehensive review of mechanisms and electrochemical performance", Applied Sciences **15** (2025) 3335. https://doi.org/10.3390/app15063335.

[11] J. E. Álvarez-Ley, R. I. Méndez-Novelo, G. Giácoman-Vallejos, L. A. Paniagua Solar & L. San-Pedro, "Microbial fuel cells for power generation and wastewater treatment: A review of components, performance and sustainability", International Journal of Hydrogen Energy **137** (2025) 429. https://doi.org/10.1016/j.ijhydene.2025.05.140.

[12] M. Verma & V. Mishra, "Recent trends in upgrading the performance of yeast as electrode biocatalyst in microbial fuel cells", Chemosphere **284** (2021) 131383. https://doi.org/10.1016/j.chemosphere.2021.131383.

[13] H. Huang, Y. Yang, S. Yang, X. Yang, Y. Huang, M. Dong, S. Zhou & M. Xu, "Filamentous electroactive microorganisms promote mass transfer and sulfate reduction in sediment microbial electrochemical systems", Chemical Engineering Journal **466** (2023) 143214. https://doi.org/10.1016/j.cej.2023.143214.

[14] S. Saadia, B. Houcine, B. Abdelhak & M. Ahmed, "Optimization of factors affecting biogas production from dairy wastewater using response surface methodology and its kinetic and microbial analysis", Results in Engineering **26** (2025) 104781. https://doi.org/10.1016/j.rineng.2025.104781.

[15] T. Ngoc-Dan Cao, S.-S. Chen, H.-M. Chang, S. Sinha Ray, F. I. Hai, T. Xuan Bui & H. Mukhtar, "Simultaneous hexavalent chromium removal, water reclamation and electricity generation in osmotic bio-electrochemical system", Separation and Purification Technology **263** (2021) 118155. https://doi.org/10.1016/j.seppur.2020.118155.

[16] S. Szakács, E. O. Martínez, L. Koók, G. M. Santos, J. T. Alarcon, D. Jeison, Z. Pientka, N. Nemestóthy, K. Bélafi-Bakó & P. Bakonyi, "Biofouling-focused assessment of a novel, cellulose-based ionogel membrane applied in a microbial fuel cell", Bioresource Technology Reports **26** (2024) 101817. https://doi.org/10.1016/j.biteb.2024.101817.

[17] P. G. Zadeh, S. Rezania, M. Fattahi, P. Dang, Y. Vasseghian & T. M. Aminabhavi, "Recent advances in microbial fuel cell technology for energy generation from wastewater sources", Process Safety and Environmental Protection **189** (2024) 425. https://doi.org/10.1016/j.psep.2024.06.077.

[18] A. Colombo, A. Schievano, S. P. Trasatti, R. Morrone, N. D'Antona & P. Cristiani, "Signal trends of microbial fuel cells fed with different food-industry residues", International Journal of Hydrogen Energy **42** (2017) 1841. https://doi.org/10.1016/j.ijhydene.2016.09.069.

[19] B. Christgen, M. Spurr, E. M. Milner, P. Izadi, C. McCann, E. Yu, T. Curtis, K. Scott & I. M. Head, "Does pre-enrichment of anodes with acetate to select for Geobacter spp. enhance performance of microbial fuel cells when switched to more complex substrates?", Frontiers in Microbiology **14** (2023) 1199286. https://doi.org/10.3389/fmicb.2023.1199286.

[20] S. Thakur, R. K. Calay, M. Y. Mustafa, F. E. Eregno & R. R. Patil, "Importance of substrate type and its constituents on overall performance of microbial fuel cells", Current Research in Biotechnology **9** (2025) 100272. https://doi.org/10.1016/j.crbiot.2025.100272.

[21] Z. Lin, S. Cheng, Y. Sun, H. Li & B. Jin, "Realizing BOD detection of real wastewater by considering the bioelectrochemical degradability of organic pollutants in a bioelectrochemical system", Chemical Engineering Journal **444** (2022) 136520. https://doi.org/10.1016/j.cej.2022.136520.

[22] G. Wei, T. Wei, Z. Li, C. Wei, Q. Kong, X. Guan, G. Qiu, Y. Hu, C. Wei, S. Zhu, Y. Liu & S. Preis, "BOD/COD ratio as a probing index in the O/H/O process for coking wastewater treatment", Chemical Engineering Journal **466** (2023) 143257. https://doi.org/10.1016/j.cej.2023.143257.

[23] L. R. B. Rebello, T. Siepman & S. Drexler, "Correlations between TDS and electrical conductivity for high-salinity formation brines characteristic of South Atlantic pre-salt basins", Water SA **46** (2020) 1. https://doi.org/10.17159/wsa/2020.v46.i4.9073.

[24] N. Skibbe, T. Günther, K. Schwalfenberg, R. Meyer, A. Reckhardt, J. Greskowiak, G. Massmann & M. Müller-Petke, "Comparison of methods measuring electrical conductivity in coastal aquifers", Journal of Hydrology **643** (2024) 131905. https://doi.org/10.1016/j.jhydrol.2024.131905.

[25] S. Niju, V. Shruthi & K. Priyadharshini, "Comprehensive insights into biological and bio-electrochemical treatment of the sago industry wastewater: Challenges and future perspectives", Sustainable Chemistry for the Environment **10** (2025) 100242. https://doi.org/10.1016/j.scenv.2025.100242.

[26] W. Zhao, X. Chen, H. Ma, D. Li, H. Yang, T. Hu, Q. Zhao, J. Jiang & L. Wei, "Impact of co-substrate molecular weight on methane production potential, microbial community dynamics, and metabolic pathways in waste activated sludge anaerobic co-digestion", Bioresource Technology **400** (2024) 130678. https://doi.org/10.1016/j.biortech.2024.130678.

[27] A. Castellano-Hinojosa, M. J. Gallardo-Altamirano, C. Pozo, A. González-Martínez, J. González-López & I. P. G. Marshall, "Salinity levels influence treatment performance and the activity of electroactive microorganisms in a microbial fuel cell system for wastewater treatment", Journal of Environmental Management **379** (2025) 124858. https://doi.org/10.1016/j.jenvman.2025.124858.

[28] A. Yousefi, S. Elmarhoum, S. Khodabakhshaghdam, K. Ako & G. Hosseinzadeh, "Study on the impact of temperature, salts, sugars and pH on dilute solution properties of Lepidium perfoliatum seed gum", Food Science & Nutrition **10** (2022) 3955. https://doi.org/10.1002/fsn3.2991.

[29] M. Al-Ani, A. Al-Ardah, M. Kuna, Z. Smati, A. Mohamed, M. Sliem & N. Al-Qahtani, "Analyzing small-particle contamination in disposable food service ware, drinking water, and commercial table salt in Doha, Qatar", in *ICAET 2025*, MDPI, 2025, p. 5. https://doi.org/10.3390/materproc2025022005.

[30] A. J. Margenot, S. J. Parikh & F. J. Calderón, "Fourier-transform infrared spectroscopy for soil organic matter analysis", Soil Science Society of America Journal **87** (2023) 1503. https://doi.org/10.1002/saj2.20583.

[31] A. Nuzzo, P. Buurman, V. Cozzolino, R. Spaccini & A. Piccolo, "Infrared spectra of soil organic matter under a primary vegetation sequence", Chemical and Biological Technologies in Agriculture **7** (2020) 6. https://doi.org/10.1186/s40538-019-0172-1.

[32] P. K. Krivoshein, D. S. Volkov, O. B. Rogova & M. A. Proskurnin, "FTIR photoacoustic and ATR spectroscopies of soils with aggregate size fractionation by dry sieving", ACS Omega **7** (2022) 2177. https://doi.org/10.1021/acsomega.1c05702.

[33] S. Pärnpuu, A. Astover, T. Tõnutare, P. Penu & K. Kauer, "Soil organic matter qualification with FTIR spectroscopy under different soil types in Estonia", Geoderma Regional **28** (2022) e00483. https://doi.org/10.1016/j.geodrs.2022.e00483.

[34] Y. Tkachenko & P. Niedzielski, "FTIR as a method for qualitative assessment of solid samples in geochemical research: A review", Molecules

27 (2022) 8846. https://doi.org/10.3390/molecules27248846.
[35] F. Jamoteau, M. Kansiz, M. Unger & M. Keiluweit, "Probing mineral-organic interfaces in soils and sediments using optical photothermal infrared microscopy", Environmental Science & Technology **59** (2025) 501. https://doi.org/10.1021/acs.est.4c09258.
[36] J. Wang, K. Ren, Y. Zhu, J. Huang & S. Liu, "A review of recent advances in microbial fuel cells: Preparation, operation, and application", BioTech **11** (2022) 44. https://doi.org/10.3390/biotech11040044.
[37] J. Cheng, S. Li, X. Yang, X. Huang, Z. Lu, J. Xu & Y. He, "Regulating the dechlorination and methanogenesis synchronously to achieve a win-win remediation solution for γ-hexachlorocyclohexane polluted anaerobic environment", Water Research **203** (2021) 117542. https://doi.org/10.1016/j.watres.2021.117542.
[38] A. A. Pilarska, T. Kulupa, A. Kubiak, A. Wolna-Maruwka, K. Pilarski & A. Niewiadomska, "Anaerobic digestion of food waste: A short review", Energies **16** (2023) 5742. https://doi.org/10.3390/en16155742.
[39] F. Liu, Y. Zhang, Y. Zhang, J. Yang, W. Shen, S. Yang, Z. Quan, B. Liu, Z. Yuan & Y. Zhang, "Thermodynamic restrictions determine ammonia tolerance of functional floras during anaerobic digestion", Bioresource Technology **391** (2024) 129919. https://doi.org/10.1016/j.biortech.2023.129919.
[40] A. A. Tiareti, M. Matsumura, T. Hidaka, F. Nishimura, Y. Nomura & T. Fujiwara, "Effect of oxidation reduction potential on methane emission from anaerobic septic systems", Waste Management Bulletin **3** (2025) 58. https://doi.org/10.1016/j.wmb.2024.12.003.
[41] W. Xue, W. Chanamarn, A. S. Tabucanon, S. G. Cruz & Y. Hu, "Treatment of agro-food industrial waste streams using osmotic microbial fuel cells: Performance and potential improvement measures", Environmental Technology & Innovation **27** (2022) 102773. https://doi.org/10.1016/j.eti.2022.102773.
[42] N. Stepanov, O. Senko, A. Aslanli, O. Maslova & E. Efremenko, "Enhanced biogas production from glucose and glycerol by artificial consortia of anaerobic sludge with immobilized yeast", Fermentation **11** (2025) 352. https://doi.org/10.3390/fermentation11060352.
[43] R. Agrahari, B. Bayar, H. N. Abubackar, B. S. Giri, E. R. Rene & R. Rani, "Advances in the development of electrode materials for improving the reactor kinetics in microbial fuel cells", Chemosphere **290** (2022) 133184. https://doi.org/10.1016/j.chemosphere.2021.133184.
[44] W. Zhao, T. Hu, H. Ma, D. Li, Q. Zhao, J. Jiang & L. Wei, "A review of microbial responses to biochar addition in anaerobic digestion system: Community, cellular and genetic level findings", Bioresource Technology **391** (2024) 129929. https://doi.org/10.1016/j.biortech.2023.129929.
[45] T. Yamashita, T. Hasegawa, Y. Hayashida, K. Ninomiya, S. Shibata, K. Ito, H. Mizuguchi & H. Yokoyama, "Energy savings with a biochemical oxygen demand (BOD)- and pH-based intermittent aeration control system using a BOD biosensor for swine wastewater treatment", Biochemical Engineering Journal **177** (2022) 108266. https://doi.org/10.1016/j.bej.2021.108266.
[46] A. Aiwonegbe, O. Adeyemi & F. Akhidenor, "Physico-chemical, heavy metal, and microbiological analysis of effluent from a confectionery company in Lagos State, Nigeria", African Scientific Reports **4** (2025) 333. https://doi.org/10.46481/asr.2025.4.3.333.
[47] A. D. Grossman, Y. Z. Belete, S. Boussiba, U. Yogev, C. Posten, F. Ortiz Tena, L. Thomsen, S. Wang, A. Gross, S. Leu & R. Bernstein, "Advanced near-zero waste treatment of food processing wastewater with water, carbon, and nutrient recovery", Science of the Total Environment **779** (2021) 146373. https://doi.org/10.1016/j.scitotenv.2021.146373.
[48] F. A. Aguilar-Aguilar, V. Y. Mena-Cervantes, F. S. Mederos-Nieto, G. Pineda-Flores, S. S. Morales-García & R. Hernández-Altamirano, "Biochemical methane potential of coyol fruit as a substrate for biogas production through mixture design and kinetic modeling", Biomass and Bioenergy **193** (2025) 107571. https://doi.org/10.1016/j.biombioe.2024.107571.
[49] Y. Suteja, I. G. N. P. Dirgayusa, S. G. Purnama & A. I. S. Purwiyanto, "From sea to table: Assessing microplastic contamination in local and non-local salt in Bali, Indonesia", Chemosphere **374** (2025) 144192. https://doi.org/10.1016/j.chemosphere.2025.144192.
[50] J. M. Sonawane, R. Mahadevan, A. Pandey & J. Greener, "Recent progress in microbial fuel cells using substrates from diverse sources", Heliyon **8** (2022) e12353. https://doi.org/10.1016/j.heliyon.2022.e12353.
[51] P. Winaikij, P. Sreearunothai & K. Sombatmankhong, "Probing mechanisms for microbial extracellular electron transfer (EET) using electrochemical and microscopic characterisations", Solid State Ionics **320** (2018) 283. https://doi.org/10.1016/j.ssi.2018.02.044.
[52] R. Zhang, W. Dai, H. Xiang, J. Chen, T. Yi, J. Li, J. Zhang, Q. Yang, R. Xiao & X. Li, "Characteristics and driving factors of power generation performance in microbial fuel cells: An analysis based on the CNKI database", Frontiers in Microbiology **16** (2025) 1620539. https://doi.org/10.3389/fmicb.2025.1620539.
[53] R. B. McCleskey, C. A. Cravotta, M. P. Miller, F. Tillman, P. Stackelberg, K. J. Knierim & D. R. Wise, "Salinity and total dissolved solids measurements for natural waters: An overview and a new salinity method based on specific conductance and water type", Applied Geochemistry **154** (2023) 105684. https://doi.org/10.1016/j.apgeochem.2023.105684.
[54] B. M. Saalidong, S. A. Aram, S. Otu & P. O. Lartey, "Examining the dynamics of the relationship between water pH and other water quality parameters in ground and surface water systems", PLOS ONE **17** (2022) e0262117. https://doi.org/10.1371/journal.pone.0262117.
[55] A. Barroso, T. Valente, A. P. Marinho Reis & I. M. H. R. Antunes, "A new acidity-based approach for estimating total dissolved solids in acidic mining influenced water", Water **15** (2023) 2995. https://doi.org/10.3390/w15162995.
[56] Y.-T. Zhang, Y. Zhang & L. Peng, "Electrochemical fluorescence microscopy reveals insignificant long-range extracellular electron transfer in Shewanella oneidensis anodic processes", Electrochimica Acta **398** (2021) 139305. https://doi.org/10.1016/j.electacta.2021.139305.
[57] H. Zhu, Y. Lv, M. Liu & C. Zhou, "An ORP prediction model for acid wastewater sulfidation process based on improved extreme learning machine", Computers & Chemical Engineering **194** (2025) 108998. https://doi.org/10.1016/j.compchemeng.2025.108998.
[58] K. A. K. Y. Johnston, M. Van Lankveld, R. De Rink, A. R. Mol, K. J. Keesman & C. J. N. Buisman, "Influence of oxidation-reduction potential and pH on polysulfide concentrations and chain lengths in the biological desulfurization process under haloalkaline conditions", Water Research **259** (2024) 121795. https://doi.org/10.1016/j.watres.2024.121795.
[59] M. Jamei, I. Ahmadianfar, X. Chu & Z. M. Yaseen, "Prediction of surface water total dissolved solids using hybridized wavelet-multigene genetic programming: New approach", Journal of Hydrology **589** (2020) 125335. https://doi.org/10.1016/j.jhydrol.2020.125335.
[60] G. Bampos, Z. Gargala, I. Apostolopoulos & G. Antonopoulou, "Electrochemical characteristics of microbial fuel cells operating with various food industry wastewaters", Processes **12** (2024) 1244. https://doi.org/10.3390/pr12061244.